## Formation of nano-CdS solid solution: A mechanism for Cd enrichment in sphalerite

LEI YAN<sup>1,2</sup>, YU FAN<sup>1,2</sup>, JUN HUANG<sup>3,\*,‡</sup>, TONG ZUO<sup>3</sup>, FANGYUE WANG<sup>1,2</sup>, AND TAOFA ZHOU<sup>1,2</sup>

<sup>1</sup>Ore Deposit and Exploration Center, School of Resources and Environmental Engineering, Hefei University of Technology, Hefei 230009, China

<sup>2</sup>Anhui Province Engineering Research Center for Mineral Resources and Mine Environments, Hefei 230009, China
<sup>3</sup>School of Materials Science and Engineering, Hefei University of Technology, Hefei 230009, China

#### ABSTRACT

The occurrence and mechanisms behind the supernormal enrichment of dispersed elements in sphalerite remain controversial. In this study, laser ablation inductively coupled plasma mass spectrometry (LA-ICP-MS) and scanning transmission electron microscopy (STEM) were employed to investigate the occurrence state and enrichment mechanism of cadmium (Cd) in Cd-rich sphalerite from the Jinding deposit. In regions with relatively low Cd concentrations (~4000 to 10 000 ppm), Cd was observed to substitute for Zn within the sphalerite lattice. However, in regions with high Cd concentrations (exceeding 30 000 ppm), a novel nanoscale occurrence state of Cd was identified, specifically as a nano-CdS solid solution. This finding provides new nanoscale mineralogical evidence to refine the understanding of the supernormal enrichment process of Cd in sphalerite. The enrichment of Cd is driven by mechanisms such as reactivation and dynamic recrystallization induced by plastic deformation in sphalerite, as well as solid solution precipitation during cooling. A coherent interface relationship between CdS and ZnS plays a critical role in the formation and stabilization of the nano-CdS solid solution. The formation of such nano solid solutions may represent a potential mechanism for the supernormal enrichment of dispersed elements, offering new insights into the complex distribution characteristics of these elements at the micrometer scale.

Keywords: Sphalerite, cadmium, occurrence state, enrichment mechanism, nano-CdS solid solution

## Introduction

Sphalerite is a common metallic mineral in hydrothermal deposits and often contains various dispersed elements such as cadmium, gallium, germanium, and indium (Cook et al. 2009; Ye et al. 2011; Frenzel et al. 2016). In recent years, the investigation of the occurrence state and enrichment mechanism of dispersed elements in sphalerite at the nanoscale has become a research hotspot. Techniques such as transmission electron microscopy (TEM), laser-induced breakdown spectroscopy (LIBS), and atom probe tomography (APT) have been employed to elucidate these aspects. For example, the discovery of Ge-containing nanoparticles, dynamic recrystallization and self-organization models (Cugerone et al. 2020; Fougerouse et al. 2023; Sun et al. 2023), and the phase re-equilibration of indium during diffusion processes (Xu et al. 2021) have been proposed as potential enrichment mechanisms.

Cadmium (Cd) is a typical dispersed element with an abundance of only around 0.18 ppm in the crust (Schulz et al. 2017), while its enrichment in the lattice of sphalerite is typically 10<sup>3</sup> to 10<sup>4</sup> times higher than its crustal abundance (Schwartz 2000; Ye et al. 2012). In some lead-zinc deposits with supernormal cadmium enrichment, the Cd content in sphalerite can exceed 10 wt%. For example, in the Bernic Lake deposit in

Canada and the Baisoara deposit in Romania, the Cd contents in sphalerite reach as high as 17.6 and 13.2 wt%, respectively (Černý and Harris 1978; Cook et al. 2009). Alternatively, Cd can occur in the form of greenockite inclusions within Cd-rich sphalerite (Ye et al. 2012).

The Jinding Mississippi Valley Type (MVT) lead-zinc deposit in Yunnan, China, is known to contain ~170 000 tonnes of metallic Cd with ore grades ranging from 0.01 to 0.2 wt% (Xue et al. 2007). Electron probe microanalysis (EPMA) has revealed that Cd content in sphalerite can reach up to 8.67 wt% (Duan et al. 2023), indicating that the Jinding deposit is also a typical deposit with supernormal enrichment of Cd. The formation of CdS nanoparticles and the process of supernormal Cd enrichment in Jinding sphalerite have been explained by a coupled dissolution-reprecipitation (CDR) model proposed by Duan et al. (2023). Nevertheless, it is important to note that not all Cd-rich regions (with Cd contents exceeding 30 000 ppm) in sphalerite are necessarily a result of CdS nanoparticles. In this study, a completely new occurrence state of Cd, namely "nano-CdS solid solution," was discovered in Cd-rich sphalerite in the Jinding deposit. The formation mechanism of nano-CdS solid solution is significantly different from the CDR. This finding may enrich the understanding of the mechanisms of supernormal enrichment of dispersed elements in sphalerite, provide new nanoscale mineralogical evidence for refining the process of extraordinary Cd enrichment, and offer new insights for explaining the complex distribution characteristics of dispersed elements at the micrometer scale.

<sup>\*</sup> Co-corresponding author E-mails: fanyu@hfut.edu.cn, j.huang@hfut.edu.cn † Open access: Article available to all readers online under the following license terms: MSA rights usage.

<sup>‡</sup> Present address: No. 193, Tunxi Road, Baohe District. Hefei 230009, Anhui Province China

#### **METHODS**

#### LA-ICP-MS

The analysis of trace element contents in sphalerite and mapping were conducted by LA-ICP-MS in the Ore Deposit and Exploration Center (OEDC), School of Resources and Environmental Engineering, Hefei University of Technology. The analyses were carried out on an Agilent 7900 Quadrupole ICP-MS coupled to a Photon Machines Analyte HE 193-nm ArF Excimer Laser Ablation system. The procedures and operating conditions were the same as those described by Wang et al. (2018) and Ning et al. (2017).

Each spot analysis was performed with a uniform spot size of 40  $\mu m$  in diameter at 8 Hz, with an energy of 4 J/cm². Each time-resolved analysis data consisted of a 20 s blank signal and a 40 s sample signal. The trace element contents in minerals were quantitatively calculated using multiple reference glasses (SRM-610, SRM-612, BCR-2G) as external standards without internal standards. The LA-ICP-MS mapping adopted a line scan method, with a beam spot size of 40  $\mu m$  and a scan speed of 40  $\mu m$ /s. Each line was parallel to the laser ablation spot and had the same size. The ablation frequency was 10 Hz, and the laser ablation energy was 2–3 J/cm². Background signals were collected for 20 s before and after the sample analysis.

Data analysis was performed using the internally developed software spotanalysis based on Matlab (Wang et al. 2018; Xiao et al. 2018). Instrument signal drift and background subtraction were automatically handled by the software throughout the entire analysis process. Accurate content correction was performed using the 100% normalization method for element content calculation.

#### TEM/STEM-EDS

The thin sections for the TEM study were prepared by cutting sphalerite from the Jinding deposit using a FIB-SEM dual-beam system. The sampling location is shown in Figure 1b. The sampling process is illustrated in Online Materials <sup>1</sup> Figure S1, and the sample was ultimately thinned to meet the requirements of TEM/STEM experiments, as shown in Online Materials <sup>1</sup> Figure S1d. The FIB-SEM dual-beam system (ZEISS Crossbeam 550L) is equipped with EDS and EBSD probes and can scan up to nanometer resolution.

The TEM resolution is  $\leq\!0.6$  nm at an acceleration voltage of 30 kV, and the voltage ranges from  $\geq\!20$  V to 30 kV, with continuous adjustments available. The

STEM instrument used is a 200 kV aberration-corrected transmission electron microscope (model JEM-NOEARM) equipped with a cold field emission gun and a high-order aberration corrector and TEM/STEM/EDS 3D reconstruction system, which is used for atomic-scale observation and analysis. The TEM resolution is  $\leq 0.078$  nm (200 kV), and the area of the spectroscopic system is 200 mm², with a resolution of  $\geq 133\,$  eV. Diffraction measurements were carried out by using software Digital Micrograph 3.21. Data from the American Mineralogist Crystal Structure Database (Downs and Hall-Wallace 2003) were used for indexing the electron diffraction patterns.

### RESULTS

#### Analysis of trace elements in disseminated sphalerite

Sphalerite is distributed throughout the entire mineralization process of the Jinding deposit (Deng et al. 2017; Wang et al. 2018). According to the structural types of the ore, sphalerite can be subdivided into vein, colloform, and disseminated forms, with disseminated sphalerite being the richest in Cd (Yang 2020). In the disseminated sphalerite ore of the Jinding deposit, sphalerite and galena occur as fine-grained (with a grain size of about 1 mm) subhedral and anhedral crystal (Fig. 1a). Sphalerite grains often contain small inclusions of galena, pyrite, and chalcopyrite (Fig. 1b). Trace element analysis of Cd in sphalerite using LA-ICP-MS shows Cd contents ranging from 13 900 to 40 513 ppm, with an average of 29 878 ppm (Online Materials¹ Table S1). Mapping results reveal the irregular distribution of Cd within sphalerite (Fig. 1c).

Nano-sampling was conducted using focused ion beam (FIB) at the location within sphalerite that is rich in Cd and free of inclusions. The sampling location cut through both Cd-rich and Cd-poor areas of sphalerite (Fig. 1c), for subsequent comparative STEM analysis. At the nanoscale, there is a clear boundary

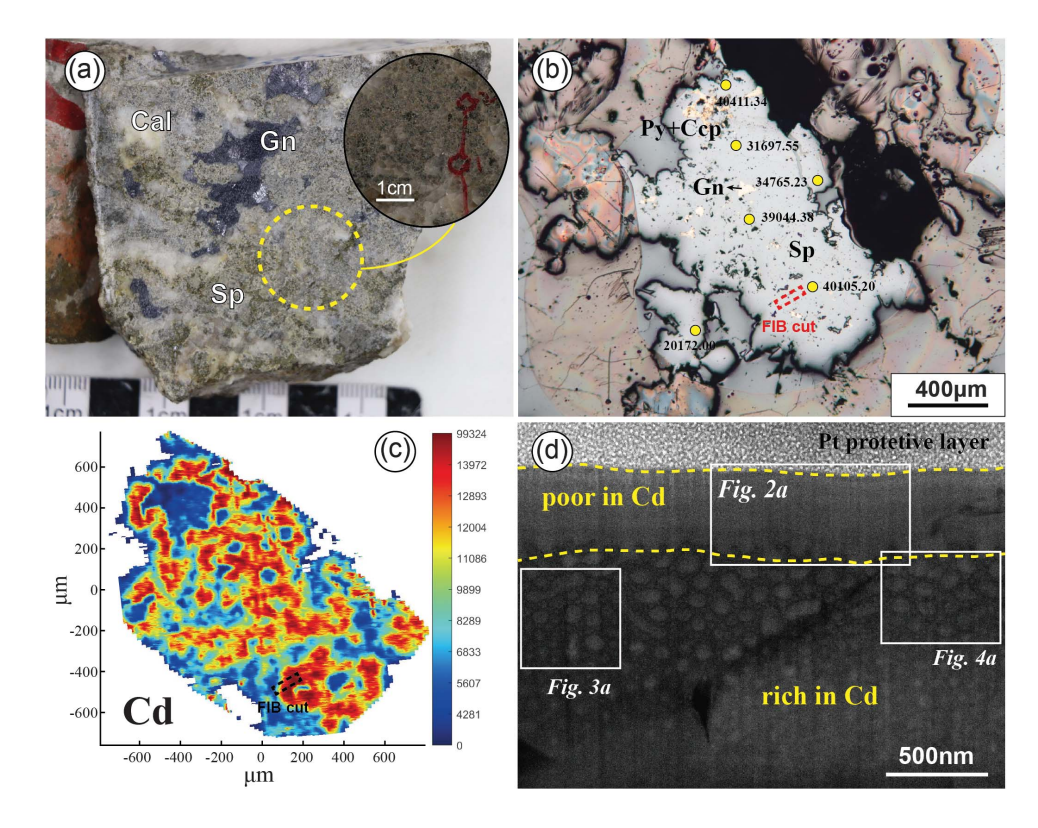


FIGURE 1. (a) Photograph of disseminated sphalerite from Jinding deposit. (b) Microscope reflected light image of sphalerite (numbers indicate Cd content results from LA-ICP-MS point analysis, in ppm) and FIB sampling position. (c) LA-ICP-MS mapping showing the distribution of Cd in the sphalerite from (b). (d) Dark-field STEM image of the thin foil sample.

between the Cd-poor and Cd-rich areas, with the former exhibiting a homogeneous feature overall, while the latter showing numerous circular to elliptical nanoscale protrusions (hereinafter referred to as nano-protrusions) (Fig. 1d).

# The occurrence state of Cd in the Cd-poor area of sphalerite

The microstructure of the Cd-poor area of sphalerite appears homogeneous overall (Fig. 2a). In high-resolution images, the arrangement of atoms is consistent with that of standard ZnS crystal structure, with almost no lattice defects observed (Fig. 2b). The selected-area electron diffraction (SAED) pattern matches the diffraction pattern of the face-centered cubic structure of ZnS along the [101] zone axis (Fig. 2c), confirming that the main component of the Cd-poor area is ZnS. From the calculation of lattice parameters, the crystal planes containing Zn atoms are  $(11\bar{1})$ ,  $(1\bar{1}\ \bar{1})$ , and  $(20\bar{2})$ . The diffraction pattern was subjected to inverse fast Fourier transform (IFFT) using Digital Micrograph software to obtain a clearer arrangement of crystal planes (Fig. 2d). To reduce the error in calculating interplanar spacing, we selected 10 consecutive interplanar

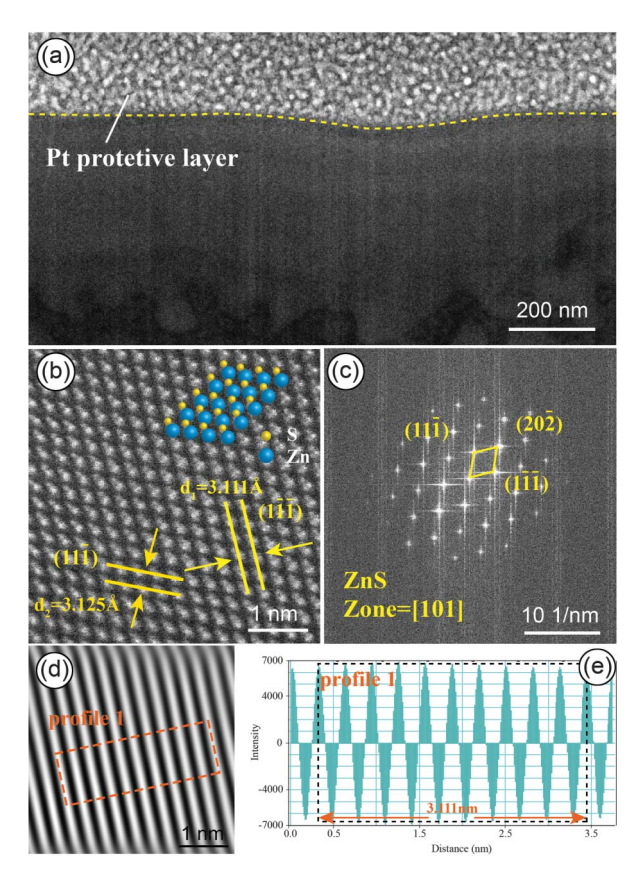


FIGURE 2. (a) HAADF-STEM image of the Cd-poor area, showing a homogeneous phase. (b) High-resolution image showing the arrangement of Zn and S atoms, consistent with the standard crystal structure of ZnS. (c) SAED pattern of (b) with lattice parameters indicated. (d) Inverse fast Fourier transform (IFFT) image of the diffraction pattern. (e) Calculation of interplanar spacing for 10 consecutive crystal planes using Digital Micrograph software.

spacings as the target, and then divided the calculation result by 10 to obtain the value of a single interplanar spacing (Fig. 2e). The interplanar spacings for  $(1\bar{1}\ \bar{1})$  are  $3.125\ Å$   $(1\ Å=0.1\ nm)$  and  $3.111\ Å$ , slightly larger than the theoretical value of  $3.070\ Å$ . Babedi et al. (2019) found that introducing Cd into the lattice sites of Zn in sphalerite resulted in a significant increase in the original Zn-S and Zn-Zn distances due to the slightly larger ionic radius of Cd<sup>2+</sup>  $(0.78\ Å)$  compared to Zn<sup>2+</sup>  $(0.60\ Å)$ . Therefore, the increased interplanar spacing in the Cd-poor area may indicate that Cd is present in sphalerite by entering the crystal lattice and occupying the sites of Zn.

## The occurrence state of Cd in the Cd-rich area of sphalerite

In the Cd-rich area of sphalerite, there are numerous nano-protrusions, with particle sizes ranging from ~20 to 100 nm. The material filling the gaps between the nano-protrusions was identified as ZnS (Figs. 3a and 4a). The distribution of Zn, S, and Cd was mapped using energy-dispersive X-ray spectroscopy (EDS) (Figs. 3b–3d), revealing the presence of CdS dispersed within the ZnS matrix. By precisely matching the bright-field image with the Cd mapping image, it was observed that Cd was locally enriched in nano-protrusions (Fig. 3d). The energy spectrum obtained from the Cd-rich area exhibits sharp peaks corresponding to Cd, Zn, and S, with no other signal peaks detected (Fig. 3e), indicating that the ZnS and CdS phases coexist within the region.

The magnified image of an individual nano-protrusion reveals that its interior may not be homogeneous (Fig. 4b). The SAED pattern obtained from FFT calibration are consistent with the diffraction pattern of face-centered cubic structure of ZnS along the zone axis [211], with crystal planes identified as  $(02\overline{2})$ ,  $(11\overline{3})$ , and  $(1\overline{1}\overline{1})$ . While along the zone axis [110], the diffraction pattern matches that of CdS, with crystal planes identified as  $(\bar{1}11)$ ,  $(\bar{2}20)$ , and  $(\bar{1}1\bar{1})$ , respectively (Fig. 3b). The IFFT image obtained from the points corresponding to CdS in the SAED pattern (indicated by arrows in the inset of Fig. 4b) shows that CdS (highlighted in yellow) is irregularly distributed in clusters within the nano-protrusions, while ZnS (highlighted in green) is distributed around it (Fig. 4c). CdS and ZnS exhibit a coherent interface relationship with continuous lattice structures (Figs. 4b and 4c). This represents a new occurrence state in sphalerite, different from isomorphic substitution and CdS nanoparticles, which we refer to as nano-CdS solid solution.

Due to the approximate square dependence of atomic brightness in high-angle annular dark-field scanning transmission electron microscopy (HAADF-STEM) images on the atomic number (Z value) squared (Jesson and Pennycook 1995; Krivanek et al. 2010; Zhao et al. 2018), and considering that the atomic number of Cd ( $Z_{\rm Cd}$  = 48) is significantly higher than that of Zn ( $Z_{\rm Zn}$  = 30), theoretically, brighter areas in the HAADF-STEM image correspond to higher Cd content. Under the assumption that sample thickness and flatness effects have been excluded, the atomic number is the sole factor influencing contrast in HAADF-STEM images. Upon closer observation at the boundary between the nano-protrusions and ZnS matrix, a noticeable contrast difference was observed, with the former appearing brighter and the latter relatively darker (Fig. 4d),

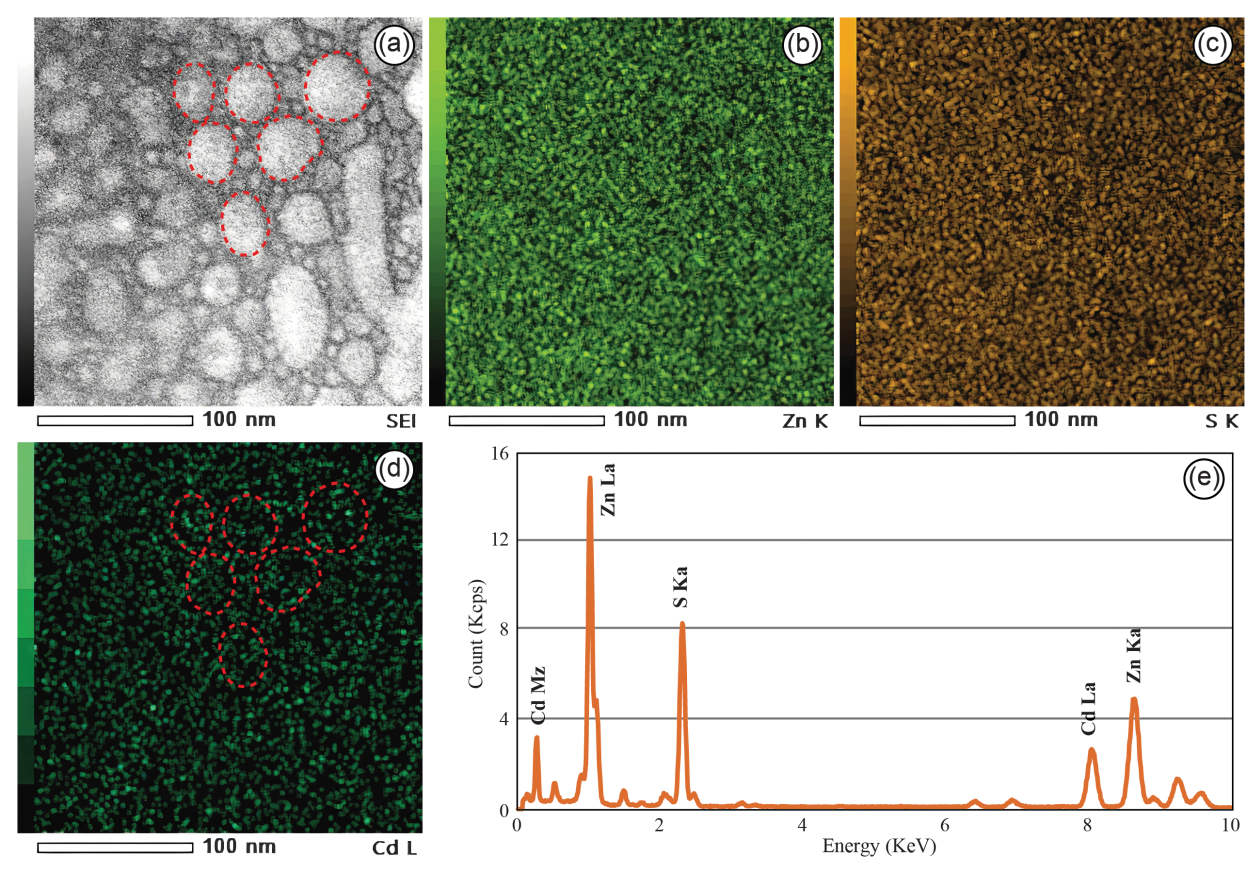


FIGURE 3. Energy-dispersive X-ray spectroscopy (EDS) mapping image and corresponding energy spectrum for the Cd-rich areas in sphalerite. (a) The secondary electron image (SEI) of the Cd-rich areas in sphalerite. (b-d) The EDS mapping images show the distribution of Zn, S, and Cd in the Cd-rich areas. Especially, the occurrence of localized enrichment of Cd within nanoscale protrusions in (d). (e) The energy spectrum of the Cd-rich areas.

suggesting a higher Cd content in the nano-protrusions. Considering the slight height difference between the nano-protrusions and ZnS matrix, although the influence of sample thickness and flatness on image contrast cannot be completely ruled out, the local enrichment of Cd in the nano-protrusions in STEM-EDS (Fig. 3d) and the sharp signal peak of Cd (Fig. 3e) further confirm the Cd-rich characteristics of the nano-protrusions. Upon closer observation of the nano-CdS solid solution and the surrounding ZnS (highlighted in the boxed area in Fig. 4c), multiple stacking faults were found at the interface positions between the two phases. When magnified to the atomic scale, they exhibited roughly parallel arrangements with significant atomic layer misalignment (Fig. 4e). These observations indicate that in Jinding sphalerite, Cd-rich areas can generate nano-CdS solid solution, making it highly detectable for the enrichment of Cd in the nanoprotrusions.

### The coherent interface relationship between CdS and ZnS

In nature, precipitate phases with different crystal structures are often found in the matrix, forming phase interfaces with the matrix phase. Based on the different lattice matching between the two phases, phase interfaces can be classified as coherent interfaces, semi-coherent interfaces, and incoherent interfaces. When the lattice matching between the two phases is optimal, meaning that the

atomic arrangement on the interface of the two different phases satisfies the lattice positions of both phases, the interface is known as a coherent interface. This type of interface demonstrates strong bonding and the capacity to accommodate deformation. In the studied Jinding sphalerite, characterization results from selected areas of the Cd-rich mineral phase revealed a significant lattice matching between the CdS phase and the ZnS matrix. From the crystal plane and atomic arrangement features (Fig. 5a), it is observed that the  $(02\overline{2})$  plane of ZnS coincides with the  $(\overline{2}20)$ plane of CdS, and the orientations of the two phases are consistent on these crystal planes, with similar interplanar spacing. The interplanar spacing of the (022) plane in ZnS is 1.88 Å according to the standard PDF card (Agrawal et al. 1994), while the interplanar spacing of the (220) plane in CdS is 2.05 Å (Yeh et al. 1992) with a difference of only 0.17 Å. Therefore, the interface between the two phases can form a good atomic matching relationship (Fig. 5b). Furthermore, the orientations of the ZnS (022) plane and the CdS (220) plane are consistent (Fig. 5c), indicating a highly similar atomic arrangement at the interface of the ZnS and CdS heterogeneous phases. This confirms the coherency between ZnS and CdS, providing further evidence for the existence of nano-CdS solid solution in the nano-protrusions of Cd-rich sphalerite. Hence, a coherent structural model has been proposed here (Fig. 5).

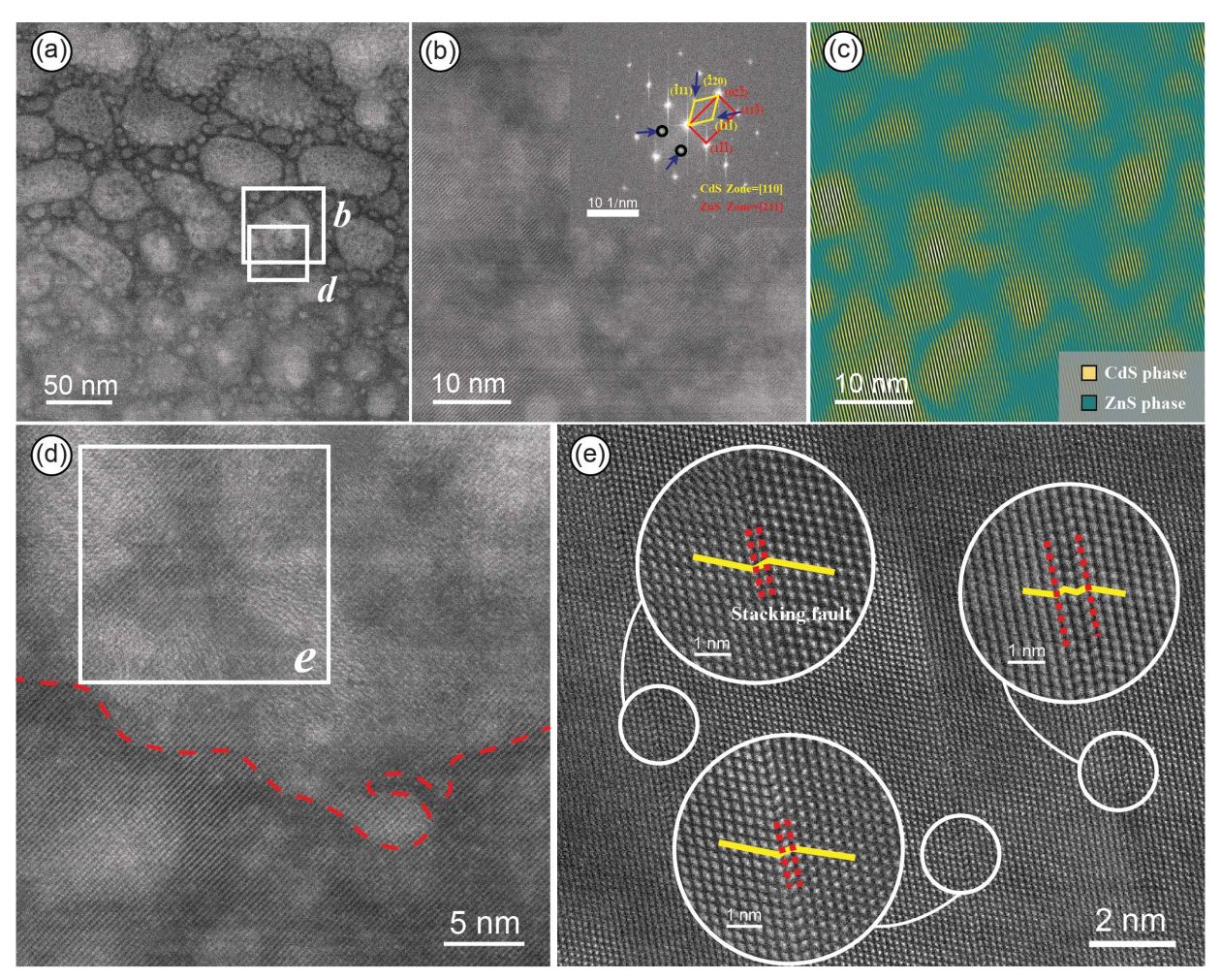


FIGURE 4. (a) HAADF-STEM image of the nano-protrusions in the Cd-rich area. (b) Magnified image of a single nano-protrusion and its corresponding SAED pattern, indicating a coherent interface relationship between ZnS and CdS. (c) IFFT image showing the distribution of CdS in the nano-protrusions, where nano-CdS solid solutions are highlighted in yellow and ZnS is highlighted in green. (d) Image cropped from (a), with dashed lines indicating the boundary between the nano-protrusions and ZnS. The nano-protrusions appear brighter, while the ZnS phase appears darker. (e) Image cropped from (c), showcasing the stacking fault structures around the nano-CdS solid solution, with the atomic arrangement magnified.

#### DISCUSSION

## The occurrence state of Cd in sphalerite

The crystal structure of sphalerite is face-centered cubic, with Zn and S in a tetrahedral coordination (Vaughan and Craig 1997). It can accommodate various dispersed elements such as Cd, Ga, Ge, and In. Currently, it is widely recognized that Cd in sphalerite exists in two main forms, isomorphic substitution and independent minerals (e.g., Ye et al. 2005; Wen et al. 2020; Li et al. 2021). The isomorphic substitution is primarily based on the relationship between the valence state, ionic radius, and abundance of elements (Liu et al. 2023). It is believed that divalent cations such as Cd directly replace Zn in the sphalerite lattice (Cd<sup>2+</sup>  $\leftrightarrow$  Zn<sup>2+</sup>), occupying the structural sites of Zn (Cook et al. 2009; Ye et al. 2011; Bonnet et al. 2016; George et al. 2016; Liu et al. 2022). The independent minerals of Cd mainly exist in sphalerite as micrometer-sized greenockite inclusions (Hu et al. 2023) or CdS nanoparticles (Duan et al. 2023).

Two different forms of Cd occurrence were discovered in the Jinding sphalerite: (1) In the relatively Cd poor areas of sphalerite (Cd content of ~4000 to 10 000 ppm), Cd entered the sphalerite structure by replacing Zn, same as the previously known isomorphic substitution  $Cd^{2+} \leftrightarrow Zn^{2+}$ . The calculated lattice parameters, which indicate an increase in the interplanar spacing of ZnS, provide strong evidence for this (Liu et al. 2023) (Fig. 2). (2) In the Cd-rich areas of sphalerite (Cd content >30 000 ppm), a new form of nanoscale Cd occurrence, nano-CdS solid solution, was found. It is distinct from both the isomorphic substitution and the greenockite nanoparticles (Bonnet et al. 2016; Duan et al. 2023). This determination was made based on SAED patterns that exhibited distinct diffraction patterns from ZnS (Fig. 4b inset), and the calculated lattice parameters that showed consistency with CdS diffraction patterns along the zone axis [110]. This confirmed the presence of an independent CdS phase, distinguishing it from the substitution of Cd for Zn in the sphalerite lattice. There are primarily two main differences between nano-CdS solid solution and CdS nanoparticles. First, the relationship between CdS and ZnS is different. The nano-CdS solid

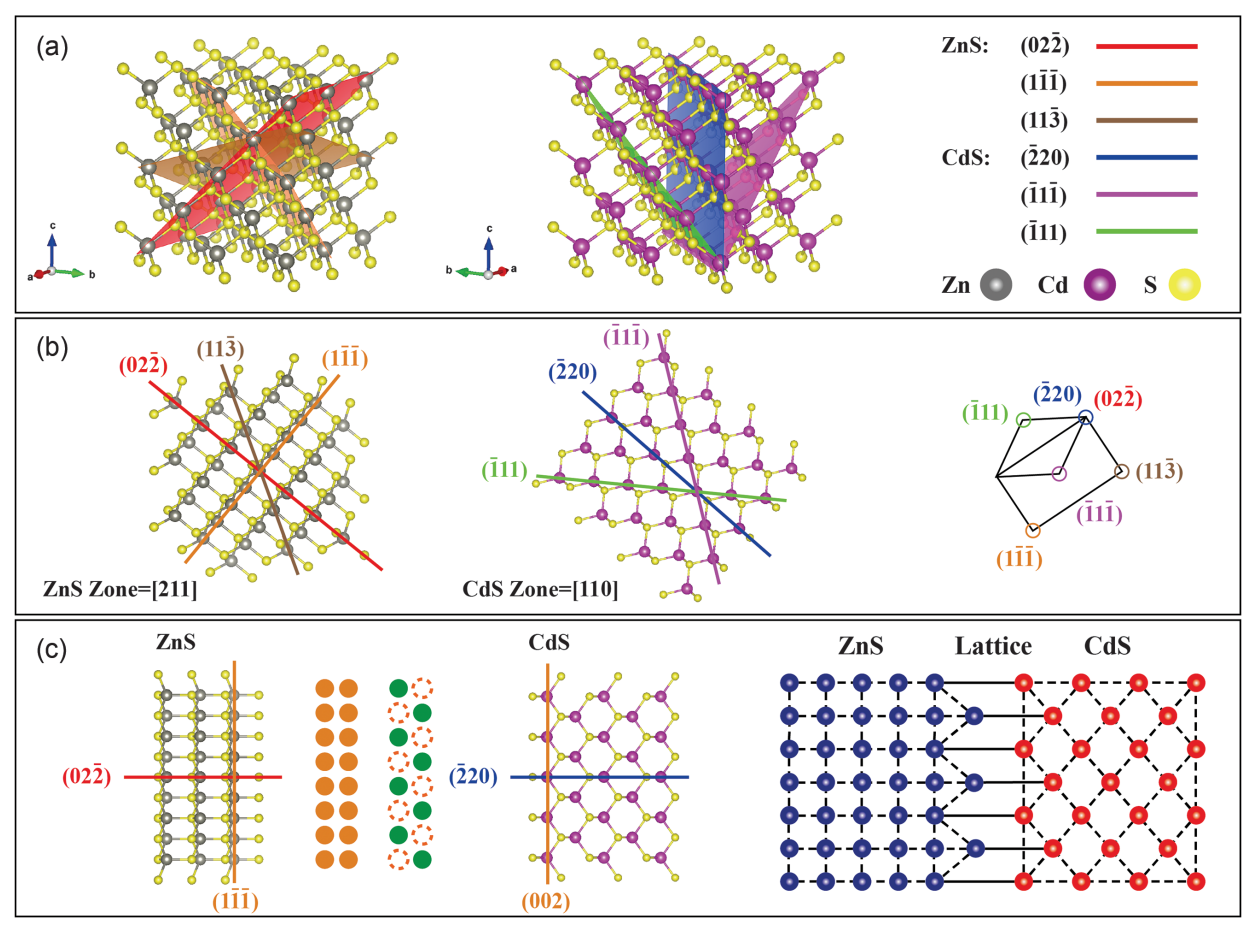


FIGURE 5. Coherent interface relationship model of nano-CdS solid solution with the ZnS matrix.

solution discovered here exhibits a coherent interface relationship with ZnS, while the CdS nanoparticles have incoherent interfaces with sphalerite (ZnS) (Duan et al. 2023). Second, their formation mechanisms are different. The CdS nanoparticles were products of coupled dissolution and reprecipitation resulting from the transient injection of low Zn/Cd residual brines into Cd-rich sphalerite (Duan et al. 2023). However, the formation of nano-CdS solid solution may involve the reactivation of Cd, dynamic recrystallization, and solid solution precipitation during the cooling process. The size of the nano-CdS solid solution ranges approximately from 2 to 12 nm (Fig. 4c), and the poor crystallinity (Fig. 4e) reflects a rapid crystallization process (Moreau et al. 2004; Myagkaya et al. 2020). This is consistent with previous experimental results of co-precipitation of CdS and ZnS and observations using TEM (e.g., Barrett and McBride 2007; Castillo et al. 2012; Xu et al. 2016; Mintcheva et al. 2019; Sakpirom et al. 2019; Smieja-Król et al. 2022).

#### Enrichment mechanism of Cd

The enrichment mechanism of Cd in ore deposits. Cd is mainly enriched in sphalerite of lead-zinc deposits. The statistical results from Schwartz (2000) indicate that there are significant differences in Cd content in sphalerite of different deposit types. Sphalerite of MVT deposits has the highest Cd content

(4850 ppm), while sphalerite of exhalative deposits has the lowest Cd content (the mean for Volcex is 2360 ppm and that for Sedex is 2560 ppm). Skarn deposits are between the two (3540 ppm). Obviously, these differences are the result of the comprehensive influence of multiple factors during the mineralization process, which are closely related to the Cd/Zn ratio in the mineralization environment, the properties of the fluid, the physical and chemical conditions (e.g., temperature, pressure, pH, etc.), and the types and quantities of ligands (e.g., Cl<sup>-</sup>, HS<sup>-</sup>, S<sup>2-</sup>) in the solution (Zhu et al. 2013). Wen et al. (2016) found that the properties of fluids and the source region of Cd are the primary factors controlling the Cd content in sphalerite through the study of stable isotopes of cadmium. The hydrothermal lead-zinc deposits in the Sichuan-Yunnan-Guizhou area of China show a pattern of Cd enrichment in sphalerite formed in relatively low temperature environments (Wen et al. 2019). In addition, the high Fe content in sphalerite may have a certain inhibitory effect on the enrichment of Cd. There is a negative correlation between Cd and Fe in sphalerite, as reported in the Fule deposit in Yunnan province and the Tianbaoshan deposit in Sichuan province (Zhu et al. 2016, 2017).

Fluid inclusions are important media for revealing the physical and chemical conditions of mineralization, the properties, and the evolution of ore-forming fluids. The observation results of the cold and hot tables of fluid inclusions in the Jinding deposit show that there is a significant decreasing trend in the homogenization temperature of fluid inclusions from the eastern (average 170 °C) to the western (average 95 °C) part of the deposit. The salinity was the opposite, increasing from an average of 8.3% in the eastern section to an average of 12.8% in the western section. The reverse trend of temperature and salinity may indicate that high-temperature and low-salinity ore-forming fluids from the deep mantle were mixed with basin fluids of low temperature and high salinity during their ascent along the migration pathway. The distribution range of hydrogen and oxygen isotopes fully confirms the occurrence of fluid mixing (Xue et al. 2017). The mixing of two fluids with different properties leads to a sudden drop in temperature, and multiple ore-forming substances such as Zn and Cd precipitate to form minerals (Xue et al. 2003). The changes in δCe and δEu of fluid inclusions reflect the transition of the fluid from weak oxidizing to reducing during the mineralization process, and the large-scale precipitation of ore-forming materials in the fluid may be related to fluid mixing or reservoir destruction (Yin et al. 1990; Xue et al. 2003). In addition, the study of the ore-forming dynamics of the Jinding deposit suggests that the ore-forming fluid has ultrahighpressure properties (up to  $170 \times 10^5$  Pa). This ultrahigh-pressure fluid exhibits periodic pulsations and has a strong ability to expand hydrothermal channels and transport minerals during active periods. During the intermission period, the reduced activity and transport capacity of fluids lead to the unloading and mineralization of ore-forming materials (Chi et al. 2012; Xue et al. 2017).

The enrichment of Cd in Jinding sphalerite may also be related to biological involvement in mineralization, as evidenced by the widespread distribution of organic matter such as asphalt, heavy oil, and carbonaceous substances in the deposit. The isotopic studies provide evidence for the biological enrichment of Cd. The  $\delta^{114/110}$ Cd composition (-0.76 ~ +0.66 %) of pyrite and sphalerite is very similar to biological samples such as algae  $(-1.01 \sim -0.86 \%)$  and flora and fauna  $(-0.79 \sim +0.64 \%)$ . The Jinding deposit also has a carbonate platform environment, suggesting that pre-enrichment of Cd in sphalerite may be achieved by algae and other organisms in shallow marine waters (Yang 2020). In addition, cadmium isotopes and sulfur isotopes of metal sulfides (such as pyrite, sphalerite, and galena) in the sphalerite of the Jinding deposit also record biological involvement in mineralization processes (Zhu et al. 2016; Huang 2019). The discovery of bacterial fossils in Jinding deposit is direct evidence of bacterial sulfide reduction (BSR) during the mineralization process, which reduces SO<sub>4</sub><sup>2-</sup> in sulfates to H<sub>2</sub>S (Machel 2001; Leach et al. 2017; Yalikun et al. 2018). BSR can provide sufficient reduced sulfur under low-temperature conditions, which is beneficial for the precipitation and mineralization of Zn and Cd.

The enrichment mechanism of Cd in sphalerite. Sphalerite is a mineral with relatively low Mohs hardness (3–4.5) and is highly prone to plastic deformation (Chen et al. 2023). Barrie et al. (2011) found that plastic deformation of sphalerite can occur at relatively low temperatures, and materials science experiments have shown that the temperature conditions for plastic deformation of cubic structured sphalerite crystals can even be as low as room temperature (Kitou et al. 2023). The stress background during the mineralization period of the Jinding deposit corresponds to transition from regional compression to strike-slip in the Lanping Basin (Wang et al. 2001; Zhang et al.

2010; Yalikun et al. 2018). The development of thrusting, folding, and secondary structures within the deposit, along with the complex and turbulent mineralization environment, can easily lead to plastic deformation of sphalerite.

The reactivation caused by plastic deformation of sphalerite is the dynamic mechanism for Cd enrichment. Under the driving force of plastic deformation, the internal kinetic energy within the sphalerite structure increased, leading to the reactivation of Cd<sup>2+</sup> from sphalerite. This resulted in the release of Cd<sup>2+</sup> from the constraints of the sphalerite lattice (Cugerone et al. 2020). Additionally, lattice defects formed during the plastic deformation of sphalerite played an important role in the recrystallization process of nanoscale protrusions. The formation processes of briartite [Cu<sub>2</sub>(Zn,Fe)GeS<sub>4</sub>] in sphalerite (Fougerouse et al. 2023) and "invisible" gold in pyrite (Fougerouse et al. 2021) both involved the participation of nanoscale lattice defects, revealing the ability of lattice defects to capture dispersed elements. Materials science experiments have shown that common elements such as B, W, Mo in nickel-based high-temperature alloys tend to segregate and accumulate at dislocations (Antonov et al. 2023; Schulz et al. 2023).

The dynamics generated during plastic deformation in the Jinding deposit led to the release of Cd from the sphalerite lattice, causing its reactivation and migration. The capturing ability of stacking faults formed during the plastic deformation of sphalerite (Fig. 4d) promoted the enrichment of Cd within them (Fig. 6b). Subsequently, under the influence of dynamic recrystallization, crystallization occurred at the stacking faults, forming Cd-enriched nano-protrusions (Fig. 6c), while the original sphalerite structure remained largely unchanged. FFT calibration results showed that the lattice parameters of the nano-protrusions and ZnS in the original sphalerite were different (Figs. 2c and 4b), indicating a change in the crystallization direction of sphalerite, which is closely related to the temperature gradient and stress field changes in the crystallization environment (Zhao et al. 2013). This further confirmed that the nano-protrusions were products of dynamic recrystallization. This process achieved the spatial redistribution of Cd, with Cd concentrated and enriched in the newly crystallized nanoprotrusions, leading to the depletion of Cd in the original sphalerite and exacerbating the uneven distribution of Cd within the sphalerite at a macroscopic level. The morphology of the nano-protrusions resembles irregular "3D island-shaped" structures formed on the growth surface via heteroepitaxial Stranski-Krastanov (SK) growth (e.g., Mo et al. 1990; Kaiser 2002), which may be related to the reduction of strain energy within the crystal (Wu et al. 2019).

The formation of nano-CdS solid solution involved the process of solid solution precipitation during cooling, where temperature played a crucial role. As the temperature decreased, the originally dispersed atoms tended to precipitate and followed the principle of minimizing energy to form coherent interfaces with the matrix. This process has been widely studied in materials science. For example, in carbon-doped high-entropy alloys, nano-precipitates containing Al, Ni, and C elements were found to be fully coherent with the matrix (Zhou et al. 2023). Moreover, in WNbMoTa-based refractory high-entropy alloys, the addition of TiNi phase resulted in the precipitation of Ni<sub>70</sub>Ti<sub>20</sub>Nb<sub>10</sub> phase that is coherent with the TiNi phase (Cai et al. 2023). All of these are related to the process of solid

solution precipitation. The characteristic of this process is that the precipitated substance is not a single phase, but a new phase formed by the combined precipitation of solute atoms with some solvent elements in the matrix phase. In geological research, similar solid-solution precipitation processes have been reported, such as the solid solution between hematite (Fe<sub>2</sub>O<sub>3</sub>) and corundum (Al<sub>2</sub>O<sub>3</sub>) (Zhao et al. 2022). Hematite and corundum have similar crystal structures, and Fe<sup>3+</sup> can easily replace Al<sup>3+</sup> in the corundum structure. However, due to the larger ionic radius of Fe<sup>3+</sup> (0.64 Å) compared to Al<sup>3+</sup> (0.51 Å), the substitution process needs to occur in a high-temperature and highpressure environment (Li et al. 2018). As corundum moves away from the mantle, temperature and pressure decrease, and unstable Fe combines with O in the corundum lattice to form hematite (Zhao et al. 2022). During the formation process of nano-CdS solid solution, Cd and ZnS act as solute atoms and solvent matrix phase, respectively. The cooling and decompression effects lead to Cd becoming supersaturated and precipitating out of ZnS. The resulting new phase is the nano-CdS solid solution that is coherent with ZnS matrix (Fig. 6d).

In crystals, if the precipitated phase has lattice parameters similar to or integer multiples of the matrix, the precipitated phase tends to exhibit a coherent interface relationship with the matrix (Quek et al. 2011). Research has shown that high lattice matching between two mineral lattices can significantly reduce interfacial energy, thereby facilitating the nucleation and growth of mineral crystals (Robinson et al. 1977). During the calibration process of the nano-protrusions, we observed that when the CdS crystallographic zone axis was [110] and the ZnS crystallographic zone axis was [211], there was an overlap in the diffraction patterns of ZnS and CdS, corresponding to the (022) plane of ZnS and the (220) plane of CdS, respectively (Fig. 4b). This indicated that the crystallographic orientation of the  $(02\bar{2})_{ZnS}$  plane and the  $(\bar{2}20)_{CdS}$  plane was similar (Fig. 5b). According to the standard PDF card (data obtained from the ICDD, Kabekkodu et al. 2024), the interplanar spacing of the  $(02\overline{2})_{ZnS}$  plane is 1.88 Å, and the interplanar spacing of the (220)<sub>CdS</sub> plane is 2.05 Å, resulting in a difference of only 0.17 Å between the two phases. In addition, the interplanar spacing of the (001)<sub>CdS</sub> plane is 2.97 Å, while the interplanar spacing of the  $(1\bar{1}\ \bar{1})_{ZnS}$  plane is 3.12 Å, with a difference of only 0.15 Å, and the orientations of these two atomic planes are also consistent. These data strongly confirm the good match between the two phases, where some atoms in CdS and ZnS can share the arrangement of atomic lattices, forming a coherent interface relationship (Fig. 6e). This relationship can reduce the interfacial energy between the nano-CdS solid solution in the nano-protrusions and the ZnS matrix. Additionally, it represents a relatively good bond between the two phases, which may be crucial for the formation and stable existence of nano-CdS solid solution in the Jinding sphalerite.

The enrichment mechanism of Cd in sphalerite. We have combined microscale LA-ICP-MS with nanoscale STEM methods to study the occurrence and enrichment mechanisms of Cd in sphalerite of other deposit types. The Xiwan deposit, located in the Middle-Lower Yangtze River Metallogenic Belt, has a variation range of Cd content in sphalerite from 2186 to 9859 ppm. The variation range of Cd content in Jinding sphalerite is 13 900~40 513 ppm (Online Materials 1 Table S1), with a

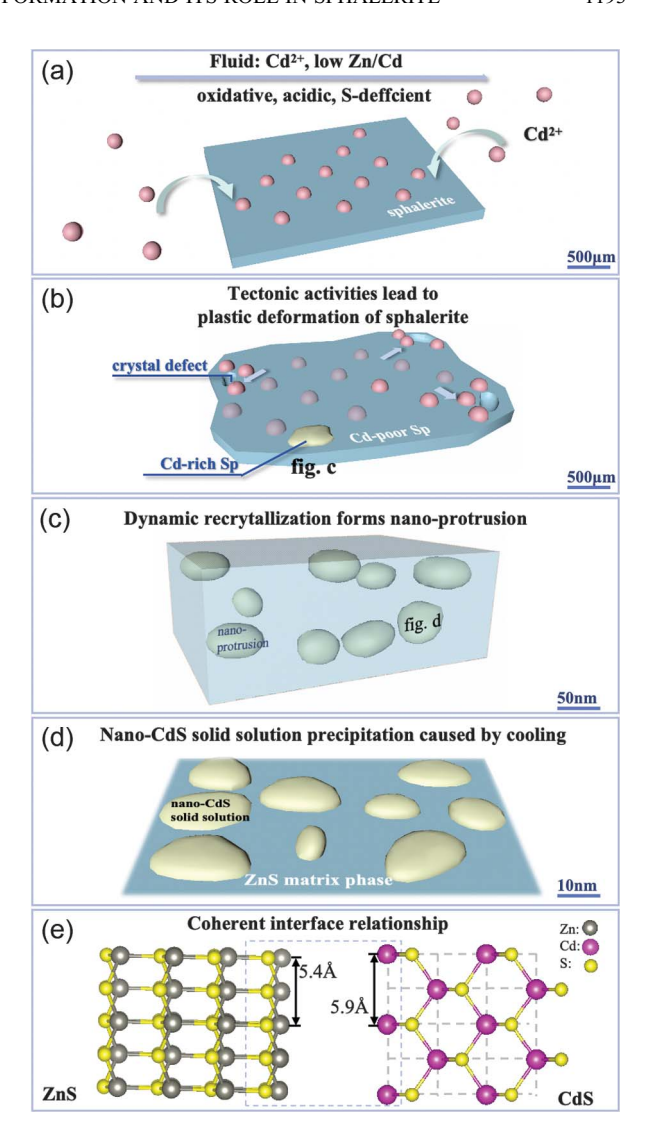


FIGURE 6. Schematic diagram showing supernormal enrichment process of Cd in sphalerite. (a) During the crystallization process of sphalerite, Cd<sup>2+</sup> in the fluid enters the lattice of sphalerite. (b) Under the stress caused by tectonic activities, plastic deformation of sphalerite occurs, creating crystal defects and triggering the activation and migration of Cd<sup>2+</sup> to accumulate at the crystal defects, forming localized Cd-rich sphalerite. (c) Cd-rich sphalerite originates from the formation of Cd-rich nano-protrusions through dynamic recrystallization. (d) Cooling leads to the precipitation of nano-CdS solid solution within the nano-protrusions. (e) Nano-CdS solid solution exhibits coherent interface relationship with the ZnS matrix.

maximum of 86 670 ppm (Duan et al. 2023). The comparative results indicate that the Cd content of sphalerite may need to exceed a certain threshold to form an independent mineral of Cd, which may range from 27 000 to 40 000 ppm, but further detailed research is still needed (Yan et al. 2024).

# Inspiration on the spatial distribution characteristics of dispersed elements

Dispersed elements such as Cd, Ge, In, and Ga are primarily enriched in lead-zinc deposits, and their heterogeneous spatial distribution poses challenges for industrial development and the utilization of these elements. In sphalerite, the main host mineral, the irregular zoning or oscillatory zoning formed by dispersed elements is often interpreted as fluctuations in the composition of hydrothermal fluids (e.g., Di Benedetto et al. 2005; Gagnevin et al. 2014; Cugerone et al. 2021) or spatial variations in crystal structure and growth rates (Pfaff et al. 2011; Luo et al. 2022). Recent studies have emphasized nanoparticles as the primary mechanism for the redistribution of dispersed elements. For example, the formation of Cd-rich nanoparticles through dissolution and reprecipitation processes (Duan et al. 2023) and the precipitation of Zn-Ge-Pb-S nanoparticles controlled by self-organization processes lead to fluctuations in the concentration of dispersed elements in the boundary layer (Sun et al. 2023).

During the ore formation process, plastic deformation of sphalerite led to the reactivation and migration of dispersed elements within the mineral. This resulted in the formation of localized enrichment areas, such as the Cd-rich nano-protrusions discussed in this study, achieving the initial enrichment of dispersed elements. Subsequently, during the cooling process, nano solid solutions precipitated, further enriching the dispersed elements. This may represent a new mechanism for the supernormal enrichment of dispersed elements in sphalerite. Nanoscale mineralogical evidence suggested that nano-CdS solid solution played a crucial role in the process of achieving Cd enrichment. This mechanism is expected not only to exist in the Jinding deposit but also potentially to operate in other MVT-type deposits. It may even be extended to explain the phenomenon of trace element enrichment in other minerals where nanoscale particles are not detected. Previous studies on the distribution characteristics of dispersed elements in host minerals have primarily relied on time-resolved depthconcentration profiles obtained through in situ quantitative microbeam techniques such as LA-ICP-MS and secondary ion mass spectrometry (SIMS) (e.g., Cook et al. 2009; Gregory et al. 2014, 2015; LaFlamme et al. 2016; Li et al. 2020) However, considering the relatively coarse spatial resolution of LA-ICP-MS and SIMS (10 µm to several tens of micrometers), it becomes challenging to accurately characterize the supernormal enrichment and complex zoning of dispersed elements, at the nanoscale, such as the nano-CdS solid solution observed in this study (ranging from a few nanometers to tens of nanometers, as shown in Fig. 4c). The formation of nano-CdS solid solution might be a potential mechanism underlying the irregular mottled enrichment of Cd at the micrometer scale in sphalerite (Fig. 1c).

## **IMPLICATIONS**

## Refinement of supernormal enrichment mechanism

The discovery of a new nanoscale occurrence state of Cd in Cd-rich sphalerite, specifically the nano-CdS solid solution, provides valuable nanoscale mineralogical evidence and refines our understanding of the supernormal enrichment process of Cd in sphalerite. By identifying the occurrence state and enrichment mechanism of Cd in different areas, this study contributes to the resolution of the controversy surrounding the occurrence state and supernormal enrichment of dispersed elements in sphalerite. Furthermore, the study highlights the importance of reactivation and dynamic recrystallization induced by plastic deformation of sphalerite, as well as

solid-solution precipitation caused by cooling, in the enrichment of Cd. These mechanisms shed light on the processes that drive the concentration and distribution of Cd in sphalerite and have implications for predicting and interpreting the enrichment patterns of dispersed elements in similar geological settings, contributing to the exploration of other systems where similar processes may occur.

#### Coherent interface relationship

The coherent interface relationship between CdS and ZnS is identified as a crucial factor for the formation and stable existence of the nano-CdS solid solution. This finding emphasizes the significance of interfacial interactions in the formation of solid solutions and their impact on the distribution and enrichment of dispersed elements. The coherent interface relationship provides insights into the formation of nano solid solution in sphalerite as a new occurrence state. The findings contribute to refining the understanding of mineral formation processes and have the potential to inform future studies on the enrichment of elements in other mineral systems.

### Expansion and limitations of research methods

In addition to identifying the occurrence and enrichment mechanisms of Cd in sphalerite, we have extended the research methods to study other dispersed elements in other minerals, such as Re in molybdenite and Co in pyrite. Although no independent mineral of Re was observed in the Merlin deposit in Australia, the presence of lattice defects such as quintuple twinning and stacking faults in molybdenite was found to be beneficial for the enrichment of Re (Yan et al. 2023). In the De'erni deposit in China, Co is present in pyrite in two forms: cobaltite nanoparticles and lattice substitution for Fe. STEM can directly observe the nanoparticles of cobaltite. However, due to the close relative atomic mass between Co and Fe in the host pyrite, the contrast difference is not significant in HAADF-STEM images, making it difficult to visually determine the specific location of Co in the pyrite lattice. The combination of LA-ICP-MS and STEM methods can effectively determine the occurrence and enrichment mechanisms of dispersed elements in most minerals. However, in some special cases, it still faces difficulties and challenges. It is necessary to comprehensively utilize multi-domain, multi-dimensional, and different resolution analysis methods for multi-scale investigations.

## ACKNOWLEDGMENTS

This work was financially supported by the National Natural Science Foundation of China (grant no. 91962218) and the National Key Research and Development Program of China (grant no. 2022YFC2903503). We would like to thank the experimenters from the Electron Microscopy Center of the Institute of Material Science and Information Technology of Anhui University for their guidance and help in FIB-SEM sample preparation and high-resolution TEM experiments.

#### REFERENCES CITED

Agrawal, B.K., Yadav, P.S., and Agrawal, S. (1994) *Ab initio* calculation of the electronic, structural, and dynamical properties of Zn-based semiconductors. Physical Review B, 50, 14881, https://doi.org/10.1103/PhysRevB.50.14881. Antonov, S., Després, A., Mayer, C., Martin, G., and Kontis, P. (2023) Boron trapping at dislocations in an additively manufactured polycrystalline superalloy. Materialia, 30, 101801, https://doi.org/10.1016/j.mtla.2023.101801.

Babedi, L., von der Heyden, B.P., Neethling, P.H., and Tadie, M. (2019) The effect of Cd-substitution on the Raman vibrational characteristics of sphalerite. Vibrational Spectroscopy, 105, 102968, https://doi.org/10.1016/j.vibspec.2019.102968.

- Barrett, K.A. and McBride, M.B. (2007) Dissolution of zinc-cadmium sulfide solid solutions in aerated aqueous suspension. Soil Science Society of America Journal, 71, 322–328, https://doi.org/10.2136/sssaj2006.0124.
- Barrie, C.D., Pearce, M.A., and Boyle, A.P. (2011) Reconstructing the pyrite deformation mechanism map. Ore Geology Reviews, 39, 265–276, https://doi.org/10.1016/j.oregeorev.2011.03.006.
- Bonnet, J., Mosser-Ruck, R., Caumon, M.C., Rouer, O., Andre-Mayer, A.S., Cauzid, J., and Peiffert, C. (2016) Trace element distribution (Cu, Ga, Ge, Cd, and Fe) in sphalerite from the Tennessee MVT deposits, USA, by combined EMPA, LA-ICP-MS, Raman spectroscopy, and Crystallography. Canadian Mineralogist, 54, 1261–1284, https://doi.org/10.3749/canmin. 1500104.
- Cai, J.L., Zhang, H., Wang, L., Sun, X.Y., Xu, X.B., Guo, X., and Li, D.C. (2023) Design and coherent strengthening of ultra-high strength refractory high entropy alloys based on laser additive manufacturing. Materials Science and Engineering A, 886, 145681, https://doi.org/10.1016/j.msea.2023.145681.
- Castillo, J., Pérez-López, R., Caraballo, M.A., Nieto, J.M., Martins, M., Costa, M.C., Olías, M., Cerón, J.C., and Tucoulou, R. (2012) Biologically-induced precipitation of sphalerite-wurtzite nanoparticles by sulfate-reducing bacteria: Implications for acid mine drainage treatment. The Science of the Total Environment, 423, 176–184, https://doi.org/10.1016/j.scitotenv.2012.02.013.
- Černý, P. and Harris, D.C. (1978) The Tanco pegmatite at Bernic Lake, Manitoba. XI. Native elements, alloys, sulfides and sulfosalts. Canadian Mineralogist, 16, 625–640.
- Chen, Y.H., Lan, T.G., Tang, Y.W., Liu, L., Hu, H.L., Wang, H., and Xu, Y. (2023) LA-ICP-MS analysis of single fluid inclusions in sphalerite and its implications: A case study from Xintianling tungsten deposit in Nanling region, South China. Mineralium Deposita, 42, 859–876 (in Chinese with English abstract).
- Chi, G.X., Xue, C.J., Qing, H.R., Xue, W., Zhang, J.W., and Sun, Y.Q. (2012) Hydrodynamic analysis of clastic injection and hydraulic fracturing structures in the Jinding Zn- Pb deposit, Yunnan, China. Geoscience Frontiers, 3, 73–84, https://doi.org/10.1016/j.gsf.2011.07.003.
- Cook, N.J., Ciobanu, C.L., Pring, A., Skinner, W., Shimizu, M., Danyushevsky, L., Saini-Eidukat, B., and Melcher, F. (2009) Trace and minor elements in sphalerite: A LA-ICPMS study. Geochimica et Cosmochimica Acta, 73, 4761–4791, https://doi.org/10.1016/j.gca.2009.05.045.
- Cugerone, A., Cenki-Tok, B., Oliot, E., Muñoz, M., Barou, F., Motto-Ros, V., and Le Goff, E. (2020) Redistribution of germanium during dynamic recrystallization of sphalerite. Geology, 48, 236–241, https://doi.org/10.1130/G46791.1.
- Cugerone, A., Cenki-Tok, B., Munoz, M., Kouzmanov, K., Oliot, E., Motto-Ros, V., and Le Goff, E. (2021) Behavior of critical metals in metamorphosed Pb-Zn ore deposits: Example from the Pyrenean Axial Zone. Mineralium Deposita, 56, 685–705, https://doi.org/10.1007/s00126-020-01000-9.
- Deng, J., Wang, C.M., Bagas, L., Selvaraja, V., Jeon, H., Wu, B., and Yang, L.F. (2017) Insights into ore genesis of the Jinding Zn-Pb deposit, Yunnan Province, China: Evidence from Zn and in-situ S isotopes. Ore Geology Reviews, 90, 943–957, https://doi.org/10.1016/j.oregeorev.2016.10.036.
- Di Benedetto, F., Bernardini, G.P., Costagliola, P., Plant, D., and Vaughan, D.J. (2005) Compositional zoning in sphalerite crystals. American Mineralogist, 90, 1384–1392, https://doi.org/10.2138/am.2005.1754.
- Downs, R.T. and Hall-Wallace, M. (2003) The American Mineralogist Crystal Structure Database. American Mineralogist, 88, 247–250.
- Duan, H.Y., Wang, C.M., Hu, R., Zhu, J.X., and Deng, J. (2023) Supernormal enrichment of cadmium in sphalerite via coupled dissolution-reprecipitation process. Communications Earth & Environment, 4, 356, https://doi.org/10. 1038/s43247-023-01025-8.
- Fougerouse, D., Reddy, S.M., Aylmore, M., Yang, L., Guagliardo, P., Saxey, D.W., Rickard, W.D.A., and Timms, N. (2021) A new kind of invisible gold in pyrite hosted in deformation-related dislocations. Geology, 49, 1225–1229, https://doi.org/10.1130/G49028.1.
- Fougerouse, D., Cugerone, A., Reddy, S.M., Luo, K., and Motto-Ros, V. (2023) Nanoscale distribution of Ge in Cu-rich sphalerite. Geochimica et Cosmochimica Acta, 346, 223–230, https://doi.org/10.1016/j.gca.2023.02.011.
- Frenzel, M., Hirsch, T., and Gutzmer, J. (2016) Gallium, germanium, indium, and other trace and minor elements in sphalerite as a function of deposit type — A meta-analysis. Ore Geology Reviews, 76, 52–78, https://doi.org/10.1016/j. oregeorev.2015.12.017.
- Gagnevin, D., Menuge, J.F., Kronz, A., Barrie, C., and Boyce, A.J. (2014) Minor elements in layered sphalerite as a record of fluid origin, mixing, and crystallization in the Navan Zn-Pb ore deposit, Ireland. Economic Geology and the Bulletin of the Society of Economic Geologists, 109, 1513–1528, https://doi.org/10.2113/econgeo.109.6.1513.
- George, L.L., Cook, N.J., and Ciobanu, C.L. (2016) Partitioning of trace elements in co-crystallized sphalerite-galena-chalcopyrite hydrothermal ores. Ore Geology Reviews, 77, 97–116, https://doi.org/10.1016/j.oregeorev.2016.02.009.
- Gregory, D., Meffre, S., and Large, R. (2014) Comparison of metal enrichment in pyrite framboids from a metal-enriched and metal-poor estuary. American Mineralogist, 99, 633–644, https://doi.org/10.2138/am.2014.4545.
- Gregory, D., Large, R., Halpin, J.A., Baturina, E.L., Lyons, T.W., Wu, S., Danyushevsky, L., Sack, P.J., Chappaz, A., Maslennikov, V.V., and others. (2015) Trace element content of sedimentary pyrite in black shales. Economic

- Geology and the Bulletin of the Society of Economic Geologists, 110, 1389–1410, https://doi.org/10.2113/econgeo.110.6.1389.
- Hu, R., Duan, H.Y., Yang, X.Z., Yang, L.F., Li, Q.X., and Wang, C.M. (2023) Occurrence of rare-dispersed element Cd in the Jinding lead-zinc-cadmiumthallium deposit, and its ore genesis. Mineral Exploration, 14, 1350–1366 (in Chinese with English abstract).
- Huang, S.Q. (2019) Interaction between hydrocarbon fluids and host rocks/evaporites in the Jinding world-class Zn-Pb deposit: Implication for ore genesis, 25–80. Ph.D. thesis, China University of Geosciences (Beijing) (in Chinese with English abstract).
- Jesson, D.E. and Pennycook, S.J. (1995) Incoherent imaging of crystals using thermally scattered electrons. The Royal Society Proceedings: Mathematical and Physical Sciences, 449, 273–293.
- Kabekkodu, S., Dosen, A., and Blanton, T. (2024) PDF-5+: a comprehensive Powder Diffraction File™ for materials characterization. Powder Diffraction, 39(2), 47–59, https://doi.org/10.1017/S0885715624000150.
- Kaiser, N. (2002) Review of the fundamentals of thin-film growth. Applied Optics, 41, 3053–3060, https://doi.org/10.1364/AO.41.003053.
- Kitou, S., Oshima, Y., Nakamura, A., Matsunaga, K., and Sawa, H. (2023) Room-temperature plastic deformation modes of cubic ZnS crystals. Acta Materialia, 247, 118738, https://doi.org/10.1016/j.actamat.2023.118738.
- Krivanek, O.L., Chisholm, M.F., Nicolosi, V., Pennycook, T.J., Corbin, G.J., Dellby, N., Murfitt, M.F., Own, C.S., Szilagyi, Z.S., Oxley, M.P., and others. (2010) Atom-by-atom structural and chemical analysis by annular dark-field electron microscopy. Nature, 464, 571–574, https://doi.org/10. 1038/nature08879.
- LaFlamme, C., Martin, L., Jeon, H., Reddy, S.M., Selvaraja, V., Caruso, S., Bui, T.H., Roberts, M.P., Voute, F., Hagemann, S., and others. (2016) In situ multiple sulfur isotope analysis by SIMS of pyrite, chalcopyrite, pyrrhotite, and pentlandite to refine magmatic ore genetic models. Chemical Geology, 444, 1–15, https://doi.org/10.1016/j.chemgeo.2016.09.032.
- Leach, D.L., Song, Y.C., and Hou, Z.Q. (2017) The world-class Jinding Zn-Pb deposit: Ore formation in an evaporite dome, Lanping Basin, Yunnan, China. Mineralium Deposita, 52, 281–296, https://doi.org/10.1007/s00126-016-0668-6.
- Li, C., Habler, G., Griffiths, T., Rečnik, A., Jeřábek, P., Götze, L.C., Mangler, C., Pennycook, T.J., Meyer, J., and Abart, R. (2018) Structure evolution of h.c.p./ c.c.p. metal oxide interfaces in solid-state reactions. Acta Crystallographica. Section A, Foundations and Advances, 74, 466–480, https://doi.org/10.1107/ S205327331800757X.
- Li, Z.L., Ye, L., Hu, Y.S., Wei, C., Huang, Z.L., Yang, Y.L., and Danyushevsky, L. (2020) Trace elements in sulfides from the Maozu Pb-Zn deposit, Yunnan Province, China: Implications for trace-element incorporation mechanisms and ore genesis. American Mineralogist, 105, 1734–1751, https://doi.org/10.2138/am-2020-6950.
- Li, K.X., Leng, C.B., Ren, Z., Liu, F., Xu, D.R., Ye, L., and Luo, T.Y. (2021) Progresses of researches on the dispersed elements associated with lead-zinc deposits. Acta Mineralogica Sinica, 41, 225–233 (in Chinese with English abstract). Liu, Y.C., Hou, Z.Q., Yue, L.L., Ma, W., and Tang, B.L. (2022) Critical metals in
- Liu, Y.C., Hou, Z.Q., Yue, L.L., Ma, W., and Tang, B.L. (2022) Critical metals in sediment-hosted Pb-Zn deposits in China. Kexue Tongbao, 67, 406–424, https://doi.org/10.1360/TB-2021-0838 (in Chinese with English abstract).
- Liu, W.H., Mei, Y., Etschmann, B., Glenn, M., MacRae, C.M., Spinks, S.C., Ryan, C.G., Brugger, J., and Paterson, D.J. (2023) Germanium speciation in experimental and natural sphalerite: Implications for critical metal enrichment in hydrothermal Zn-Pb ores. Geochimica et Cosmochimica Acta, 342, 198–214, https://doi.org/10.1016/j.gca.2022.11.031.
- Luo, K., Cugerone, A., Zhou, M.F., Zhou, J.X., Sun, G.T., Xu, J., He, K.J., and Lu, M.D. (2022) Germanium enrichment in sphalerite with acicular and euhedral textures: An example from the Zhulingou carbonate-hosted Zn(-Ge) deposit, South China. Mineralium Deposita, 57, 1343–1365, https://doi.org/10.1007/s00126-022-01112-4.
- Machel, H.G. (2001) Bacterial and thermochemical sulfate reduction in diagenetic settings—Old and new insights. Sedimentary Geology, 140, 143–175, https:// doi.org/10.1016/S0037-0738(00)00176-7.
- Mintcheva, N., Gicheva, G., Panayotova, M., Wunderlich, W., Kuchmizhak, A.A., and Kulinich, S.A. (2019) Preparation and photocatalytic properties of CdS and ZnS nanomaterials derived from metal xanthate. Materials, 12, 3313, https://doi.org/10.3390/ma12203313.
- Mo, Y., Savage, D.E., Swartzentruber, B.S., and Lagally, M.G. (1990) Kinetic pathway in Stranski-Krastanov growth of Ge on Si(001). Physical Review Letters, 65, 1020–1023, https://doi.org/10.1103/PhysRevLett.65.1020.
- Moreau, J.W., Webb, R.I., and Banfield, J.F. (2004) Ultrastructure, aggregation-state, and crystal growth of biogenic nanocrystalline sphalerite and wurtzite. American Mineralogist, 89, 950–960, https://doi.org/10.2138/am-2004-0704.
- Myagkaya, I.N., Lazareva, E.V., Zaikovskii, V.I., and Zhmodik, S.M. (2020) Interaction of natural organic matter with acid mine drainage: Authigenic mineralization (case study of Kursk sulfide tailings, Kemerovo region, Russia). Journal of Geochemical Exploration, 211, 106456, https://doi.org/10.1016/j.gexplo.2019.106456.
- Ning, S.Y., Wang, F.Y., Xue, W.D., and Zhou, T.F. (2017) Geochemistry of the Baoshan pluton in the Tongling region of the Lower Yangtze River Belt. Geochimica, 46, 397–412, https://doi.org/10.19700/j.0379-1726.2017.05.001 (in Chinese with English abstract).

- Pfaff, K., Koenig, A., Wenzel, T., Ridley, I., Hildebrandt, L.H., Leach, D.L., and Markl, G. (2011) Trace and minor element variations and sulfur isotopes in crystalline and colloform ZnS: Incorporation mechanisms and implications for their genesis. Chemical Geology, 286, 118-134, https://doi.org/10. 1016/j.chemgeo.2011.04.018.
- Quek, S.S., Xiang, Y., and Srolovitz, J.D. (2011) Loss of interface coherency around a misfitting spherical inclusion. Acta Materialia, 59, 5398-5410, https://doi.org/10.1016/j.actamat.2011.05.012.
- Robinson, P., Ross, M., Nord, G.L., Smyth, J.R., and Jaffe, H.W. (1977) Exsolution lamellae in augite and pigeonite; fossil indicators of lattice parameters at high temperature and pressure. American Mineralogist, 62, 857-873
- Sakpirom, J., Kantachote, D., Siripattanakul-Ratpukdi, S., McEvoy, J., and Khan, E. (2019) Simultaneous bioprecipitation of cadmium to cadmium sulfide nanoparticles and nitrogen fixation by Rhodopseudomonas palustris TN110. Chemosphere, 223, 455–464, https://doi.org/10.1016/j.chemosphere.2019.02.051.
- Schulz, K.J., DeYoung, J.H. Jr., Seal, R.R. III, and Bradley, D.C. (2017) Critical Mineral Resources of the United States-Economic and Environmental Geology and Prospects for Future Supply, 868 p. U.S. Geological Survey.
- Schulz, B., Haghdadi, N., Leitner, T., Hafok, M., and Primig, S. (2023) Dynamic recrystallisation via nucleation at distorted twins in a Ni-based superalloy. Journal of Alloys and Compounds, 936, 168318, https://doi.org/10.1016/j. jallcom, 2022, 168318.
- Schwartz, M.O. (2000) Cadmium in zinc deposits: Economic geology of a polluting element. International Geology Review, 42, 445-469, https://doi.org/10. 1080/00206810009465091.
- Smieja-Król, B., Pawlyta, M., and Gałka, M. (2022) Ultrafine multi-metal (Zn, Cd, Pb) sulfide aggregates formation in periodically water-logged organic soil. The Science of the Total Environment, 820, 153308, https://doi.org/10. 1016/j.scitotenv.2022.153308.
- Sun, G.T., Zhou, J.X., Cugerone, A., Zhou, M.F., and Zhou, L.L. (2023) Germanium-rich nanoparticles in Cu-poor sphalerite: A new mechanism for Ge enrichment. GSA Bulletin, 136, 2891–2905. https://doi.org/10.1130/B37014.1. Vaughan, D.J. and Craig, J.R. (1997) Sulfide ore mineral stabilities, morphologies,
- and intergrowth textures. Geochemistry of Hydrothermal Ore Deposits, 367-434.
- Wang, J.H., Yin, A., Harrison, T.M., Grove, M., Zhang, Y.Q., and Xie, G.H. (2001) A tectonic model for Cenozoic igneous activities in the eastern Indo-Asian collision zone. Earth and Planetary Science Letters, 188, 123-133, https://doi.org/10.1016/S0012-821X(01)00315-6.
- Wang, C.M., Yang, L.F., Bagas, L., Evans, N.J., Chen, J.Y., and Du, B. (2018) Mineralization processes at the giant Jinding Zn-Pb deposit, Lanping Basin, Sanjiang Tethys Orogen: Evidence from in situ trace element analysis of pyrite and marcasite. Geological Journal, 53, 1279-1294, https://doi.org/10.1002/gj.2956.
- Wen, H., Zhu, C., Zhang, Y., Cloquet, C., Fan, H., and Fu, S. (2016) Zn/Cd ratios and cadmium isotope evidence for the classification of lead-zinc deposits. Scientific Reports, 6, 25273, https://doi.org/10.1038/srep25273.
- Wen, H.J., Zhou, Z.B., Zhu, C.W., Luo, C.G., Wang, D.Z., Du, S.J., Li, X.F., Chen, M.H., and Li, H.Y. (2019) Critical scientific issues of super-enrichment of dispersed metals. Yanshi Xuebao, 35, 3271-3291, https://doi.org/10. 18654/1000-0569/2019.11.01 (in Chinese with English abstract).
- Wen, H.J., Zhu, C.W., Du, S.J., Fan, Y., and Luo, C.G. (2020) Gallium (Ga), germanium (Ge), thallium (Tl) and cadmium (Cd) resources in China. Kexue Tongbao, 65, 3688-3699, https://doi.org/10.1360/TB-2020-0267 (in Chinese with English abstract).
- Wu, Y.F., Fougerouse, D., Evans, K., Reddy, S.M., Saxey, D.W., Guagliardo, P., and Li, J.W. (2019) Gold, arsenic, and copper zoning in pyrite: A record of fluid chemistry and growth kinetics. Geology, 47, 641-644, https://doi.org/ 10.1130/G46114.1.
- Xiao, X., Zhou, T.F., White, N.C., Zhang, L.J., Fan, Y., and Chen, X.F. (2018) The formation and trace elements of garnet in the skarn zone from the Xinqiao Cu-S-Fe-Au deposit, Tongling ore district, Anhui Province, Eastern China.
- Lithos, 320-303, 467–479, https://doi.org/10.1016/j.lithos.2018.01.023. Xu, J., Murayama, M., Roco, C.M., Veeramani, H., Michel, F.M., Rimstidt, J.D., Winkler, C., and Hochella, M.F. Jr. (2016) Highly-defective nanocrystals of ZnS formed via dissimilatory bacterial sulfate reduction: A comparative study with their abiogenic analogues. Geochimica et Cosmochimica Acta, 180, 1-14, https://doi.org/10.1016/j.gca.2016.02.007.
- Xu, J., Ciobanu, C.L., Cook, N.J., Slattery, A., Li, X.F., and Kontonikas-Charos, A. (2021) Phase relationships in the system ZnS-CuInS2: Insights from a nanoscale study of indium-bearing sphalerite. American Mineralogist, 106, 192-205, https://doi.org/10.2138/am-2020-7488.
- Xue, C.J., Chen, Y.C., Wang, D.H., Yang, J.M., Yang, W.G., and Zeng, R. (2003) Geology and isotopic composition of helium, neon, xenon and metallogenic age of the Jinding and Baiyangping ore deposits, northwest Yunnan, China. Science in China. Series D, Earth Sciences, 46, 789–800, https://doi.org/10. 1007/BF02879523.
- Xue, C.J., Zeng, R., Liu, S.W., Chi, G.X., Qing, H.R., Chen, Y.C., Yang, J.M., and Wang, D.H. (2007) Geologic, fluid inclusion and isotopic characteristics of the Jinding Zn-Pb deposit, western Yunnan, South China: A review. Ore Geology Reviews, 31, 337-359, https://doi.org/10.1016/j.oregeorev.2005.04.007.

- Xue, C.J., Chi, G.X., and Chen, Y.C. (2017) Characteristics of ore-forming fluid system. Jinding Giant Lead-Zinc Deposit, Yunnan, China, p. 56-79. Geology Press (in Chinese).
- Yalikun, Y., Xue, C.J., and Symons, D.T.A. (2018) Paleomagnetic age and tectonic constraints on the genesis of the giant Jinding Zn-Pb deposit, Yunnan, China. Mineralium Deposita, 53, 245–259, https://doi.org/10.1007/s00126-017-0733-9.
- Yan, L., Fan, Y., Huang, J., Li, Y.Y., Zhou, T.F., Zuo, T., Zhang, Y.F., and Xu, G.Q. (2023) Occurrence state and enrichment mechanism of rhenium in molybdenite from Merlin Deposit, Australia. Ore Geology Reviews, 162, 105693, https://doi.org/10.1016/j.oregeorev.2023.105693.
- Yan, L., Fan, Y., Huang, J., Zuo, T., and Lan, B.Y. (2024) Occurrence state and enrichment mechanism of cadmium in sphalerite of Xiwan lead-zinc deposit in Luzong basin, Anhui Province, China. Yanshi Xuebao, 40, 642-662, https:// doi.org/10.18654/1000-0569/2024.02.18 (in Chinese with English abstract).
- Yang, L. (2020) Occurrence and source of Cd elements in Jinding Pb-Zn deposit, Yunnan Province, China. Master's thesis, China University of Geosciences (Beijing), 8-66 (in Chinese with English abstract).
- Ye, L., Pan, Z.P., Li, C.Y., Liu, T.G., and Xia, B. (2005) The present situation and prospects of geochemical researches on cadmium. Acta Petrologica et Mineralogica, 24, 339-348 (in Chinese with English abstract).
- Ye, L., Cook, N.J., Ciobanu, C.L., Liu, Y.P., Zhang, Q., Liu, T.G., Gao, W., Yang, Y.L., and Danyushevskiy, L. (2011) Trace and minor elements in sphalerite from base metal deposits in South China: A LA-ICPMS study. Ore Geology Reviews, 39, 188–217, https://doi.org/10.1016/j.oregeorev.2011.03.001.
- Ye, L., Cook, N.J., Liu, T.G., Ciobanu, C.L., Gao, W., and Yang, Y.L. (2012) The Niujiaotang Cd-rich zinc deposit, Duyun, Guizhou Province, southwest China: Ore genesis and mechanisms of cadmium concentration. Mineralium Deposita, 47, 683-700, https://doi.org/10.1007/s00126-011-0386-z.
- Yeh, C., Lu, Z.W., and Zunger, A. (1992) Zinc-blende-wurtzite polytypism in semiconductors. Physical Review B, 46, 10086, https://doi.org/10.1103/ PhysRevB.46.10086.
- Yin, H.H., Fan, W.M., and Lin, G. (1990) Deep processes and mantle-crust compound mineralization in the evolution of the Lanping-Simao Mesozoic-Cenozoic Diwa basin in western Yunnan, China. Geotectonica et Metallogenia, 4, 113-124 (in Chinese with English abstract).
- Zhang, B., Zhang, J.J., and Zhong, D.L. (2010) Structure, kinematics and ages of transpression during strain-partitioning in the Chongshan shear zone, western Yunnan, China. Journal of Structural Geology, 32, 445-463, https://doi.org/ 10.1016/j.jsg.2010.02.001.
- Zhao, X.B., Gao, S.F., Yang, C.B., Zhang, J., Liu, L., Fu, H.Z., Tang, X., and Cao, L.M. (2013) Influence of crystal orientation on microstructure and mechanical properties and its control for nickel-base single crystal superalloys. Materials China, 32, 24–37 (in Chinese with English abstract).
- Zhao, X., Ning, S., Fu, W., Pennycook, S.J., and Loh, K.P. (2018) Differentiating polymorphs in molybdenum disulfide via electron microscopy. Advanced Materials, 30, 1802397, https://doi.org/10.1002/adma.201802397.
  Zhao, Q.Y., Zhao, S.R., and Xu, C. (2022) Hematite exsolutions in corundum from
- Cenozoic basalts in Changle, Shandong Province, China: Crystallographic orientation relationships and interface characters. Crystals, 12, 905, https:// doi.org/10.3390/cryst12070905.
- Zhou, X.Y., Chen, J., Ding, R.G., Wu, H.Y., Lu, S.D., He, J.H., Wang, W.L., and Pan, H.G. (2023) A novel coherent particles-reinforced FCC-based highentropy superalloy with superior high-temperature compressive properties. Materials Science and Engineering A, 872, 144947, https://doi.org/10.1016/ j.msea.2023.144947.
- Zhu, C.W., Wen, H.J., Zhang, Y., and Fan, H.F. (2016) Cadmium and sulfur isotopic compositions of the Tianbaoshan Zn-Pb-Cd deposit, Sichuan Province, China. Ore  $Geology\ Reviews, 76, 152-162, https://doi.org/10.1016/j.oregeorev. 2016.01.010.$
- Zhu, C.W., Wen, H.J., Zhang, Y.X., Fan, H.F., Fu, S.H., Xu, J., and Qin, R.T. (2013) Characteristics of Cd isotopic compositions and their genetic signifi-cance in the lead-zinc deposits of SW China. Science China. Earth Sciences, 56, 2056-2065, https://doi.org/10.1007/s11430-013-4668-4 (in Chinese with English abstract).
- Zhu, C.W., Wen, H.J., Zhang, Y.X., Fu, S.H., Fan, H.F., and Cloquet, C. (2017) Cadmium isotope fractionation in the Fule Mississippi Valley-type deposit, Southwest China. Mineralium Deposita, 52, 675-686, https://doi.org/10. 1007/s00126-016-0691-7.

Manuscript received July 4, 2024 Manuscript accepted December 12, 2024 Accepted manuscript online January 2, 2025 MANUSCRIPT HANDLED BY JIE XU

#### **Endnotes:**

<sup>1</sup>Deposit item AM-25-89524. Online Materials are free to all readers. Go online. via the table of contents or article view, and find the tab or link for supplemental materials.